Published in final edited form as:
Cancer Cell. 2012 January 17; 21(1): 66–81. doi:10.1016/j.ccr.2011.11.024.

Pericyte Depletion Results in Hypoxia-Associated Epithelial-to-Mesenchymal Transition and Metastasis Mediated by Met Signaling Pathway

Vesselina G. Cooke[1,*], **Valerie S. LeBleu**[1,*], **Doruk Keskin**[1,2], **Zainab Khan**[1], **Joyce T. O'Connell**[1], **Yingqi Teng**[1], **Michael B. Duncan**[1], **Liang Xie**[1], **Genta Maeda**[1], **Sylvia Vong**[1,2], **Hikaru Sugimoto**[1], **Rafael M. Rocha**[3], **Aline Damascena**[3], **Ricardo R. Brentani**[3], and **Raghu Kalluri**[1,2,4]

[1]Division of Matrix Biology, Department of Medicine, Beth Israel Deaconess Medical Center and Harvard Medical School, Boston, MA 02115

[2]Department of Biological Chemistry and Molecular Pharmacology, Harvard Medical School, Boston, MA 02115

[3]Department of Oncology, Hospital A. C. Camargo, National Institute of Oncogenomics, Dundacao Antonio Prudente, 01509-010, Sao Paulo, Brazil

[4]Division of Health Sciences and Technology, Harvard-Massachusetts Institute of Technology, Boston, MA 02115

Summary

The functional role of pericytes in cancer progression remains unknown. Clinical studies suggest that low numbers of vessel-associated pericytes correlated with a drop in overall survival of patients with invasive breast cancer. Using genetic mouse models or pharmacological inhibitors, pericyte depletion suppressed tumor growth but enhanced metastasis. Pericyte depletion was further associated with increased hypoxia, epithelial-to-mesenchymal transition (EMT), and Met receptor activation. Silencing of *Twist* or use of a Met inhibitor suppressed hypoxia and EMT/Met-driven metastasis. In addition, poor pericyte coverage coupled with high Met expression in cancer cells speculates the worst prognosis for patients with invasive breast cancer. Collectively, our study suggests that pericytes within the primary tumor microenvironment likely serve as important gatekeepers against cancer progression and metastasis.

Address for correspondence: Raghu Kalluri, Professor of Medicine, Harvard Medical School, Division of Matrix Biology, Department of Medicine, Beth Israel Deaconess Medical Center, Boston, MA 02115, Tel# 617-667-0629, Fax# 617-667-0645, rkalluri@bidmc.harvard.edu.

*Vesselina G. Cooke and Valerie S. LeBleu contributed equally to this manuscript

Introduction

Metastasis is the leading cause of death in cancer patients. The formation of secondary tumors or metastasis is greatly influenced by multifaceted tumor-stroma interactions, in which stromal components of the tumor microenvironment can influence the behavior of the cancer cells (Coussens et al., 2000; Joyce, 2005; Thiery, 2009). While cancer cell-autonomous changes are undoubtedly critical for cancer progression and metastasis, the functional contribution of stromal cells is still emerging.

Pericytes are an integral component of the tissue vasculature. As perivascular stromal cells, pericytes provide structural support to blood vessels and regulate tissue physiology via its influence on vascular stability (Dore-Duffy and Cleary, 2011; Kim et al., 2006). Due to their essential function in vascular development, pericytes are also speculated to play an important role in tumor angiogenesis. Angiogenesis is required for the growth of tumors, and VEGF-mediated proliferation and migration of endothelial cells is critical for the generation of new capillaries, which is further supported by the recruitment of pericytes (Raza et al., 2010). Some studies have explored strategies that target both endothelial cells and pericytes (Bergers et al., 2003; Lu et al., 2007) or pericytes alone (Lu et al., 2007; Ozerdem, 2006a) to inhibit tumor angiogenesis and tumor growth. However, clinical data correlates low pericyte coverage with poor patient prognosis (O'Keeffe et al., 2008; Stefansson et al., 2006; Yonenaga et al., 2005), and disruption of pericytes has also been suggested to enhance metastasis (Xian et al., 2006).

The growth of tumors is often associated with defective tumor vasculature that cannot keep up with the overall oxygen and metabolic needs, ultimately resulting in tumor hypoxia (Harris, 2002; Semenza, 2003). Diminished oxygen levels lead to the activation and stabilization of the transcription factor HIF1α (Pouyssegur et al., 2006), and hypoxia and HIF1α expression are correlated with poor prognosis and metastasis in cancer patients (Birner et al., 2000; Bos et al., 2003; Brizel et al., 1997; Vleugel et al., 2005). Hypoxia induces epithelial-to-mesenchymal transition (EMT) of cells specifically via Hif1α activation of the master regulator of EMT *Twist* (Sun et al., 2009; Yang et al., 2008), which is suggested to play an essential role in promoting metastasis (Yang et al., 2004).

Met, the receptor for hepatocyte growth factor (HGF), is also a key promoter of EMT (Birchmeier et al., 2003). Furthermore, the *Met* promoter contains HIF1α binding sites and is regulated by both hypoxia and HIF1α (Hara et al., 2006; Hayashi et al., 2005; Pennacchietti et al., 2003). HGF/Met expression is also upregulated in many cancers (Di Renzo et al., 1991), correlating with disease progression and metastasis (Di Renzo et al., 1995; Kenworthy et al., 1992) (Natali et al., 1993).

Using genetically engineered mouse models (GEMMs) and pharmacological targeting of pericytes, we examined whether pericyte deficiency positively or negatively affects metastasis and explored possible underlying mechanisms.

Results

Low pericyte coverage is associated with invasive breast cancer and correlates with decreased patient survival

Pericyte coverage of the tumor vasculature was evaluated in tissue samples from breast cancer patients with invasive ductal carcinoma via immunostaining for NG2, a vascular pericytes marker (Bergers and Song, 2005; Jain, 2003; Ozerdem et al., 2002; Schlingemann et al., 1990; Sennino et al., 2007), and CD31, a marker for endothelial cells (Newman, 1994). The percentage of $CD31^+$ vessels associated with NG2 staining was quantified using morphometric analysis. Among various clinical characteristics, low pericyte coverage was significantly associated with the presence of distant metastasis (Table S1). Moreover, the degree of pericyte coverage also significantly correlated with disease progression and overall survival (Figure S1A). Patients with no detectable pericyte coverage on tumor vessels exhibited a shorter disease-free survival and lower rate of overall survival than patients with greater pericyte coverage.

Pericyte depletion inhibited tumor growth but produced defective tumor vasculature and increased metastasis

To functionally assess the role of pericytes in tumor progression and metastasis, we generated transgenic mice that express viral thymidine kinase (tk) under control of the *NG2* promoter (NG2-tk mice) (Figure S1B). Ganciclovir (GCV) treatment of NG2-tk mice resulted in the selective ablation of proliferating $NG2^+$ cells due to incorporation of GCV nucleoside analog during replication leading to irreversible DNA synthesis arrest. To assess the specificity of the *NG2* promoter for expression in $NG2^+$ cells, we generated NG2-YFP transgenic mice that express yellow fluorescent protein (YFP) under the control of the same *NG2* promoter sequence and found that NG2-YFP expression colocalized with NG2 antibody staining in 4T1 mammary tumors (Figure S1B–C). To determine the efficacy of the NG2-tk transgene, *in vitro* culture of $NG2^+$ cells from NG2-tk and wildtype (WT) mice were treated with varying GCV concentrations (Figure S1D). Dose-dependent ablation of $NG2^+$ cells was observed, with 75% ablation at 500 μM GCV.

4T1-GFP cancer cells were implanted into the mammary fat pad of NG2-tk mice and wildtype littermates. Primary tumor growth was monitored and daily GCV injections were initiated when tumors reached ~500 mm^3 and continued until tumors reached ~2000 mm^3 (Figure 1A). Tumor volumes decreased upon initiation of GCV treatment in the NG2-tk mice and remained significantly smaller until the experimental endpoint (Figure 1B). The number of $NG2^+$ cells, $CD31^+$ cells, and percent vessel-associated $NG2^+$ cells in the primary tumors of NG2-tk+GCV mice were significantly reduced when compared to control GCV-treated wildtype littermates (WT+GCV mice) (Figure 1C). To investigate whether pericyte depletion was associated with vascular abnormalities, we infused tumor-bearing mice with FITC-conjugated dextran and observed a greater amount of extravascular FITC-dextran in pericyte-depleted tumors (Figure 1D).

While pericyte ablation reduced primary tumor growth, 4T1 tumor-bearing NG2-tk+GCV mice exhibited increased lung metastasis when compared to WT+GCV mice (Figure 1E).

FACS and quantitative PCR analysis of genomic DNA for the cancer cell-associated *GFP* gene revealed that the number of circulating cancer cells and metastatic cancer cells in the lungs was greater in NG2-tk+GCV mice than in WT+GCV mice. Reduced tumor size and increased metastasis were also observed when pericytes were ablated in the MMTV-PyMT spontaneous mammary tumor model using GCV-treated MMTV-PyMT/NG2-tk double transgenic mice (Figure 1F–G). However, upon intravenous injection of 4T1 cancer cells into NG2-tk+GCV and WT+GCV mice, pericyte ablation had no significant effects on metastasis in the absence of a primary tumor (Figure S1E).

PDGFRβ has also been used as a marker to identify pericytes (Dore-Duffy, 2008; Hellstrom et al., 1999; Liebner et al., 2000; Ozerdem et al., 2001a; Xian et al., 2006) To validate the pro-metastatic effects of pericyte depletion observed in NG2-tk+GCV mice, we generated PDGFRβ-tk mice in which viral thymidine kinase is expressed under the *PDGFR*β promoter as an alternative model for pericyte depletion (Figure S2A). To assess the specificity of the *PDGFR*β promoter, we also generated PDGFRβ-RFP mice in which red fluorescent protein (RFP) is expressed under the same *PDGFR*β promoter element (Figure S2A–B) and found that PDGFRβ-RFP expression colocalized with PDGFRβ antibody staining in 4T1 tumors. To determine the efficacy of the PDGFRβ-tk transgene, *in vitro* culture of PDGFRβ$^+$ cells from PDGFRβ-tk and WT mice were subjected to increasing concentrations of GCV (Figure S2C). Dose-dependent ablation of PDGFRβ$^+$ cells was observed, with 60% ablation at 50 μM GCV.

4T1 cancer cells were implanted into the mammary fat pad of PDGFRβ-tk mice and WT littermates. Tumor volumes decreased upon initiation of GCV treatment in PDGFRβ-tk mice and remained significantly smaller until the experimental endpoint when compared to WT+GCV mice (Figure 2A–B). However, metastasis was greatly enhanced following ablation of PDGFRβ$^+$ cells (Figure 2C). Immunostaining with PDGFRβ antibody in the tumors of PDGFRβ-tk+GCV mice revealed 80% reduction in vessel-associated PDGFRβ$^+$ cells (Figure 2D). PDGFRβ shares ~90% colocalization with NG2 on tumor vasculature (Sugimoto et al., 2006), and vessel-associated NG2$^+$ cells were also reduced by 80% in the tumors of PDGFRβ-tk+GCV mice (Figure 2D). The overall pericyte coverage (assessed by vessel-associated NG2$^+$/PDGFRβ$^+$ double-positive cells) and the number of CD31$^+$ cells were reduced in PDGFRβ-tk+GCV mice when compared to WT+GCV mice (Figure 2D).

As an alternative model for inhibiting PDGFRβ$^+$ cells, 4T1 tumor-bearing mice were treated with PDGFRβ-specific antibodies to suppress PDGFRβ activity. PDGFRβ antibody treatment significantly decreased tumor volume and increased metastatic burden (Figure 2E–F), in association with a significant reduction in the percent vessel-associated PDGFRβ$^+$ cells (Figure 2G).

Enhanced hypoxia, HIF1α expression, and EMT program in pericyte-depleted tumors

To gain insight into the molecular mechanisms associated with increased metastasis resulting from pericyte depletion, we performed gene expression profiling of tumors from NG2-tk+GCV and WT+GCV mice. We employed genealogy analysis to identify significantly upregulated genes (grouped as pathways (Table S2) and network processes (Table S3)) in NG2-tk+GCV mice when compared to WT+GCV mice. The overlapping

processes identified were 1) response to hypoxia, 2) response to stress, and 3) cell motion/migration (Table S3). Reduced pericyte coverage can decrease vessel stability and increase hypoxia (Huang et al., 2010). In concordance, pericyte depletion in the NG2-tk+GCV mice induced a gene expression profile that reflected a hypoxic state. We assessed hypoxia levels by examining pimonidazole adduct formation in the tumors of NG2-tk+GCV and WT+GCV mice and found increased hypoxic levels in the NG2-tk+GCV pericyte-depleted tumors (Figure 3A). In addition, expression of the hypoxia-inducible transcription factor HIF1α was also significantly increased in the tumors of NG2-tk+GCV mice (Figure 3B).

The exact mechanism connecting hypoxia and cancer invasiveness remains unknown; however, several have been proposed (Dachs and Tozer, 2000; Gupta and Massague, 2006; Rofstad, 2000; Yang et al., 2008). Because cell motion/migration was identified as one of the primary processes upregulated by NG2-tk+GCV tumors in the gene expression profiling analysis, we hypothesized that EMT may be a mechanism connecting hypoxia and cancer invasiveness. Further examination of the microarray data revealed that the expression of many EMT-associated genes were upregulated in NG2-tk+GCV tumors when compared to WT+GCV tumors (Table S4). To identify epithelial cells undergoing EMT, tumors from NG2-tk+GCV and WT+GCV mice were immunostained for the epithelial marker Cytokeratin-8 (CK8) and the mesenchymal marker αSMA; the number of $CK8^+/\alpha SMA^+$ double-positive cells was significantly increased in NG2-tk+GCV pericyte-depleted tumors (Figure 3C). Next, we performed quantitative RT-PCR and confirmed that expression of *CK8* was significantly downregulated, while transcription factors associated with EMT induction, such as *Twist* and *Snail*, were significantly upregulated in NG2-tk+GCV tumors (Figure 3D). Other epithelial genes such as *E-cadherin* and *α-catenin* were also downregulated, while genes driving mesenchymal phenotype such as *Slug*, *Lox* and *Fibronectin* were upregulated.

In agreement with the data from the NG2-tk+GCV mice, tumors from MMTV-PyMT/NG2-tk+GCV mice revealed increased hypoxia along with increased numbers of $CK8^+/\alpha SMA^+$ double-positive cells, reduced *E-cadherin* expression, and increased *Twist* and *Snail* expression, when compared to tumors from MMTV-PyMT/WT+GCV mice (Figure 3E–G). Tumors from PDGFRβ-tk+GCV mice also showed increased hypoxia, increased HIF1α expression, and acquisition of an EMT program shift when compared to control mice (data not shown).

The transcription factor Twist has been termed the master regulator of EMT (Yang et al., 2004). To evaluate whether inhibition of EMT via silencing of *Twist* abrogates the metastatic phenotype seen in NG2-tk+GCV mice, we orthotopically injected 4T1 cancer cells with stably-silenced *Twist* (two different clones of 4T1-twist shRNA) into NG2-tk +GCV and WT+GCV mice. Tumor volume in 4T1-twist shRNA tumor-bearing NG2-tk +GCV mice was reduced when compared to 4T1-twist shRNA tumor-bearing WT+GCV mice (Figure 4A). Moreover, metastatic burden was decreased in 4T1-twist shRNA tumor-bearing WT+GCV mice when compared to 4T1 tumor-bearing WT+GCV mice, while metastasis was further suppressed in 4T1-twist shRNA tumor-bearing NG2-tk+GCV mice (Figure 4B–E).

Met proto-oncogene activation in pericyte-depleted tumors

Quantitative RT-PCR for *Met* revealed significantly increased *Met* expression in NG2-tk +GCV tumors when compared to WT+GCV tumors (Figure 5A). Additionally, increased phosphorylation of Met was also observed in tumors from NG2-tk+GCV and MMTV-PyMT/NG2-tk+GCV mice when compared to tumors from control mice (Figure 5B–C), as well as in PDGFRβ-tk+GCV mice (data not shown).

Next, we explored whether pharmacological targeting of Met can suppress metastasis in pericyte-ablated mice. Treatment of MMTV-PyMT/NG2-tk mice with both GCV and the Met inhibitor PF2341066 completely suppressed the enhanced metastasis of MMTV-PyMT/NG2-tk mice treated with GCV alone (Figure 5D–F). The baseline lung metastasis observed in the control tumors (without pericyte depletion, hypoxia, HIF-1α expression, Met activation and EMT) did not respond to Met inhibition.

Enhanced metastasis upon pericyte targeting using pharmacological inhibitors is suppressed by concomitant Met inhibitor treatment

Many studies have reported that Imatinib (which targets pericytes via PDGFRβ) and Sunitinib (which targets both endothelial cells and pericytes via VEGFR1, VEGFR2, VEGFR3, and PDGFRβ), drugs currently in clinical use, can inhibit tumor progression (Bergers et al., 2003; Ebos et al., 2009; Lu et al., 2007; Mendel et al., 2003; Paez-Ribes et al., 2009; Pietras and Hanahan, 2005); however, there have been limited studies examining their effects on metastasis. Treatment with Sunitinib and another receptor tyrosine kinase inhibitor Sorafenib have been demonstrated to increase metastasis in animal tumor models (Ebos et al., 2009; Paez-Ribes et al., 2009); however, the molecular mechanism for which remains largely unknown. Therefore, we examined whether Imatinib and Sunitinib enhance metastasis due to mechanisms similar to shown above.

4T1 tumor-bearing mice were treated with either Imatinib or Sunitinib. Imatinib treatment reduced pericyte coverage (as determined by vessel-associated $NG2^+$/$PDGFR\beta^+$ double-positive cells) by more than 60% (Figure S3A). In concordance with previous reports (Lu et al., 2007), decreased pericyte coverage was not accompanied by net reduction of tumor vessels (Figure S3A). Quantitative RT-PCR showed negligible expression levels of *c-Kit* and *Abl1* (additional targets of Imatinib) in 4T1 tumors, and their expression remained unchanged upon Imatinib treatment (Figure S3A). Sunitinib treatment led to reduced numbers of both $NG2^+$/$PDGFR\beta^+$ double-positive cells and $CD31^+$ endothelial cells (Figure S3A).

4T1 tumor-bearing mice treated with Sunitinib exhibited reduced tumor volume and growth with increased levels of apoptosis, while Imatinib-treated tumor-bearing mice revealed similar tumor growth kinetics when compared to mice treated with PBS-vehicle (Figure 6A–C). Analysis of lungs revealed a significantly higher level of metastatic burden in both the Imatinib-treated and Sunitinib-treated groups (Figure 6D). Quantification of FITC-dextran revealed increased amount of extravascular dextran in the tumors of Imatinib-treated and Sunitinib-treated mice (Figure 6E). Furthermore, tumors in Imatinib-treated and Sunitinib-treated mice showed significant increase in hypoxia as assessed by pimonidazole staining

(Figure 6F), as well as increased expression of HIF1α (Figure 6G). Similar to results obtained with the transgenic mice, however, Imatinib or Sunitinib treatment had no significant effects on metastasis when 4T1 cells were injected intravenously (Figure S3B).

Next, we evaluated whether pharmacological targeting of pericytes also induced an EMT program in the cancer cells. Tumors from Imatinib-treated and Sunitinib-treated mice exhibited increased numbers of $CK8^+/\alpha SMA^+$ double-positive cells when compared to tumors from PBS-treated mice (Figure 6H). In addition, quantitative RT-PCR showed significant downregulation of *E-cadherin*, while *Twist* and *Snail* were upregulated (Figure 6I). To address whether inhibition of EMT can suppress the increased metastatic phenotype seen after pharmacological targeting of pericytes, mice were implanted with 4T1-twist shRNA cells and treated with Imatinib. Silencing of *Twist* was able to suppress the Imatinib-induced EMT and metastasis without significant effects on primary tumor growth (Figure S3C).

Levels of Met and phosphorylated Met were also increased in tumors of Imatinib-treated and Sunitinib-treated mice when compared to PBS-treated mice (Figure S4A–B). Tumors from PBS-treated mice showed phosphorylated Met expression predominantly in the vascular wall, while tumors from Imatinib-treated and Sunitinib-treated mice exhibited significantly higher levels of phosphorylated Met in the cancer cells. Pharmacological targeting of Met using PF2341066 inhibited the EMT program shift and suppressed metastasis in Imatinib-treated and Sunitinib-treated mice (Figure 7A–F), despite retaining the Imatinib- or Sunitinib-induced changes in vessel integrity and tumor hypoxia (Figure 7G–I). PF2341066 treatment of Imatinib-treated and Sunitinib-treated mice successfully inhibited both Met and phosphorylated Met levels (Figure S4B). Although PF2341066 is also an inhibitor of ALK (Zou et al., 2007), quantitative RT-PCR (data not shown) and immunostaining revealed that ALK was not expressed in 4T1 tumors with or without PF2341066 treatment (Figure S4C). The baseline tumor weight and lung metastasis observed in the control tumors (without pericyte deficiency, hypoxia, HIF1α expression, Met activation and EMT) did not respond to Met inhibition alone (Figure S4D).

To further investigate whether targeting pericytes leads to increased metastasis in other tumor types, we subcutaneously implanted B16F10 mouse melanoma cells into C57Bl6 mice (Figure S4E) and orthotopically implanted 786-O human renal cell carcinoma cells under the renal capsule of nude mice (Figure S4F). The mice were then treated with PBS, Sunitinib, PF2341066 or a combination of both Sunitinib and PF2341066. Sunitinib treatment led to reduced B16F10 tumor volume and weight but an increase in metastasis. Sunitinib-treated tumors also showed increase in hypoxia, phosphorylated Met, and induction of EMT. Treatment with PF2341066 did not affect primary tumor volume and weight; however, concomitant treatment with PF2341066 and Sunitinib significantly suppressed metastasis, despite hypoxia remaining high in these tumors. Similarly, mice with RCC tumors treated with Sunitinib showed increased lung metastasis, increased hypoxia, increased phosphorylated Met, and enhanced EMT program. Concomitant treatment of RCC tumor-bearing mice with Sunitinib and PF2341066 suppressed metastasis and EMT despite high levels of hypoxia. Sunitinib-treated mice intravenously injected with RCC (to bypass

the primary tumor), however, showed significantly reduced metastasis when compared to PBS-treated mice.

To explore the impact of targeting only endothelial cells on metastasis without targeting pericytes, RCC tumor-bearing mice were treated with antihuman VEGF-A blocking antibody (Bevacizumab) and 4T1 tumor-bearing mice with anti-mouse VEGF-A blocking antibody. Bevacizumab treatment led to decreased tumor volume; however, metastasis was unchanged (Figure S4G). Tumors from Bevacizumab-treated mice did not show an increase in hypoxia or Met activation (Figure S4G). 4T1 tumor-bearing mice treated with VEGF-A antibody showed reduced tumor growth and metastasis when compared to control mice (Figure S4H). Similar results were obtained when pancreatic neuroendocrine (PNET) and RCC tumor-bearing mice were treated with endogenous inhibitors of angiogenesis that target endothelial cells, such as tumstatin and endostatin (data not shown; (Xie et al., 2011).

Loss of pericytes coupled with high Met expression is associated with decreased survival of breast cancer patients

Our experiments with mice suggested that loss of pericytes leads to enhanced tumor hypoxia and metastasis via increased Met expression in cancer cells. We evaluated breast cancer samples for pericyte coverage, HIF1α expression and Met expression. Invasive ductal carcinoma (IDC) patients with high levels of HIF1α exhibited poor prognosis with diminished disease-free survival, as has been also suggested by other studies (Baba et al., 2010; Koukourakis et al., 2002; Vleugel et al., 2005). While high Met expression in cancer cells was associated with a drop in disease-free and overall survival, the coupling of poor pericyte coverage together with high Met expression correlated with an additional drop in disease-free and overall survival (Figure 8A–B). Furthermore, pericyte coverage coupled with Met expression correlated with breast cancer stage, depth of invasion, and the presence of distant metastasis (Figure 8C).

Discussion

Tumors induce angiogenesis to generate new blood vessels (Folkman, 1971; Folkman, 1974; Folkman, 1995; Hanahan and Weinberg, 2000), and pericytes are important structural and functional components of blood vessels (Dore-Duffy and Cleary, 2011). In normal tissue, pericytes play an important role in regulating the physiological function of blood vessels; however, their precise role in the context of tumor vasculature is largely unexplored. Studies related to pericyte coverage on tumor blood vessels suggest that coverage can vary; some tumor types exhibit greater pericyte coverage whereas others exhibit limited and abnormal coverage (Eberhard et al., 2000). Many studies have suggested that targeting pericytes alone or in combination with endothelial cells might be beneficial to control tumor growth (Bergers et al., 2003; Lu et al., 2010; Ozerdem, 2006a; Ozerdem, 2006b), while other studies have suggested that pericyte deficiency may facilitate cancer metastasis (Xian et al., 2006). Our preliminary clinical studies with tissue samples from patients with invasive ductal carcinoma suggested that low numbers of vessel-associated pericytes significantly correlated with poor prognosis. Therefore, in this study, we explored the function of pericytes in cancer progression and metastasis.

Tumors in mice generally do not exhibit a significant drop in pericyte coverage until they reach a very large size (unpublished data). Therefore, we used multiple transgenic and pharmacological approaches to target pericytes and achieve their loss in tumors of reasonable size. Our data demonstrated that pericyte loss increased metastasis and was further associated with emergence of tumor hypoxia and increased expression of HIF1α. It is possible that such stromal changes can cooperate with cancer cell-autonomous changes to enhance metastasis. Met expression in cancer cells is detected in many advanced stage tumors including invasive breast cancer (Garcia et al., 2007). We propose that such induction of Met expression is a result of increased tumor hypoxia, among other possible mechanisms. In support of this notion, our results show that tumors without significant levels of hypoxia exhibit negligible expression levels of Met and treatment of these tumors with a Met inhibitor has little impact on their progression.

The reason why a drug such as Sunitinib that targets both endothelial cells and pericytes leads to enhanced metastasis raises some questions. We speculate that regardless of their ability to target endothelial cells, drugs that can target pericytes in primary tumors, such as Sunitinib and Sorafenib (Ebos et al., 2009), may increase metastasis. More studies are required to clarify these observations, but our studies suggest that pericytes may serve as negative regulators of metastasis.

It is important to note that increased metastasis is associated with poor pericyte coverage in the primary tumor. However, if pericyte are targeted to mimic adjuvant therapy in the clinic, an increase in metastasis is not observed. In fact, Sunitinib treatment of mice after intravenous introduction of RCC results in decreased metastatic colonization, consistent with the clinical experience of treating RCC patients with Sunitinib as an adjuvant therapy to control metastasis (Motzer et al., 2007). Collectively, our data support the notion that Sunitinib used in the adjuvant setting possibly helps to control metastasis of certain cancers but it might lead to increased metastasis when used in the neoadjuvant setting.

One of the challenges in studying the effect of pericyte ablation on tumor growth and metastasis is that pericytes are reported to express different markers such as NG2, PDGFRβ, αSMA, desmin, RGS5 (Bergers and Song, 2005), and their expression may be tissue specific. During vascular morphogenesis, NG2 is exclusively present on pericytes (as determined by their perivascular location) (Ozerdem et al., 2001b), and NG2 and PDGFRβ share greater than 90% co-localization in the tumor microenvironment (Sugimoto et al., 2006). Additionally, NG2 and PDGFRβ have been repeatedly reported as reliable markers for pericytes (Bergers and Song, 2005; Hellstrom et al., 1999; Ozerdem et al., 2002; Schlingemann et al., 1990; Sennino et al., 2007; Xian et al., 2006). It should be noted that in our study we achieve pericyte ablation using different transgenic mouse models that use *NG2* and *PDGFR*β promoters. While many studies have demonstrated the utility of NG2 and PDGFRβ to label pericytes in the tumor, it is possible that other cells are also identified by these markers. Therefore, despite using the most useful reagents currently available, one cannot rule out the possibility of non-pericyte cells contributing to the phenotype we observe in this study. Nevertheless, our approach of using multiple distinct strategies offers some confidence that our observations are related to pericyte targeting.

Our studies demonstrated that depletion of pericytes led to diminished primary tumor growth associated with decreased microvessel density (MVD) and hypoxia. Imatinib, which did not lead to reduced MVD, nevertheless, reduced the number of vessel-associated pericytes and also led to increased hypoxia possibly due to altered vascular integrity. The differential effects on MVD in the setting of the transgenic mouse models versus Imatinib treatment raises the possibility that Imatinib targeting of PDGFRβ is subtly distinct from strategies that eliminate proliferating pericytes. We speculate that Imatinib treatment may induce an unknown pro-angiogenic response to compensate for the loss of pericytes, which may not be present in the transgenic mice. In this regard, we observed more non-vessel-associated $NG2^+$ cells in the Imatinib-treated tumors when compared to tumors from NG2-tk+GCV and PDGFRβ-tk+GCV mice (data not shown). Such cells, while not associated with vasculature, may still potentially offer paracrine support to the defective vessels in Imatinib-treated tumors, leading to vessel retention.

VEGF is a hypoxia and HIF1α-responsive gene and the pericyte-ablated tumors revealed defective vasculature associated with hypoxia, suggesting that any possible rebound angiogenic effect due to increased VEGF in these hypoxic tumors does not overcome the overall disruption of the tumor vasculature due to pericyte deletion. Interestingly, when VEGF-A is directly targeted using a mouse VEGF-A antibody in the 4T1 setting or Bevacizumab in the context of human renal cell carcinoma, tumor volume decreases due to the decrease in angiogenesis. Hypoxia, Met expression, and metastasis however, are not increased in this setting. These results suggest that targeting endothelial cells alone may leave behind vessels that are normalized (appropriately pruned), while targeting pericytes (alone or in combination with endothelial cells) leads to leaky vasculature, increased hypoxia, increased Met, increased EMT, and enhanced metastasis (Carmeliet and Jain, 2011; Tong et al., 2004).

EMT is considered to be the first step in the metastatic cascade of carcinoma cells using the same response to migrate away from the primary tumors as normal epithelial cells employ during the development (Acloque et al., 2009; Thiery et al., 2009). EMT is enhanced by hypoxia and has been implicated in tumor invasiveness (Kalluri, 2009; Kalluri and Weinberg, 2009; Thiery et al., 2009; Trimboli et al., 2008; Yang et al., 2008). Hypoxia is a classic stress-induced factor in the tumor microenvironment, and it promotes both cellular quiescence and induction of survival pathways (Xie and Huang, 2003). Hypoxia can tip a tumor to a more invasive phenotype via mechanisms of increased extracellular proteases such as MMP2 (Munoz-Najar et al., 2006), invoking induction of Met activation (Eckerich et al., 2007; Pennacchietti et al., 2003) and EMT (Chen et al., 2010; Erler et al., 2006). Our results suggest that pericyte depletion promotes leaky/hyperpermeable vessels, which may lead to increased interstitial plasma exudates, possibly increasing the concentration of plasma proteins (including albumin) in the intratumoral/interstitial region. Such increase in the intratumoral plasma volume may increase the interstitial pressure and alter fluid dynamics, which leads to compression of remaining tumor vessels and decreases the blood flow (Jain, 1987; Stohrer et al., 2000). Collectively, such changes lead to hypoxia and set in motion a series of events that lead to increased metastasis. Hypoxia-induced EMT can be prevented by Met targeting and thus our work suggests that pericyte targeting could be

combined with Met inhibitors to achieve a synergistic benefit in controlling primary tumor growth and metastasis. This notion is in agreement with previously published reports where dual inhibitors of HGF and VEGFR (XL880 and XL184) were used (Qian et al., 2009; You et al., 2011).

Patients with invasive ductal carcinoma who exhibit poor pericyte coverage coupled with high Met expression revealed a significant drop in disease-free and overall survival. Collectively, our results suggest that an analysis of pericyte coverage on tumor vessels coupled with Met expression can serve as a useful biomarker to inform patient prognosis. More in-depth clinical studies are required to further evaluate such potential clinical utility.

Experimental Procedures

Cell Lines

4T1 BALB/c mammary tumor epithelial cells, B16F10 C57Bl6 melanoma cells, and 786-O human renal cell carcinoma cells were obtained from ATCC and grown in DMEM media supplemented with 10% fetal calf serum (FCS), 100U/ml penicillin and 100U/ml streptomycin. 4T1-twist shRNA cells (clones 5 and 7, a gift from Dr. Robert Weinberg, MIT) were cultured in DMEM media supplemented with 5% heat inactivated FCS, 5% heat activated FCS, 100U/ml penicillin and 100U/ml streptomycin.

Animal Experiments and Immunohistochemistry

Generation of transgenic mice, tumor models, drug treatments, immunohistochemistry, and additional experimental procedures are described in Supplemental Experimental Procedures. All animal experiments were reviewed and approved by the Beth Israel Deaconess Medical Center Institutional of Animal Care and Use Committee.

Quantitative PCR Analysis

Expression was determined using the Applied Biosystems 7300 Sequence Detector System and SYBR green as the fluorescence reporter. Measurements were standardized to the housekeeping gene acidic ribosomal phosphoprotein PO (*ARP/36B4*). To assess the number of 4T1-GFP$^+$ cells in the lung, quantitative PCR for *GFP* was performed using genomic DNA as a template. Primer sequences are listed in Supplemental Experimental Procedures.

Clinical Study

Breast cancer patients were recruited for biopsy at the A. C. Carmargo Hospital in Sao Paulo, Brazil after approval by the institutional review board and informed consent. The analysis was performed on 130 biopsies from patients with invasive ductal carcinoma (IDC). The tissue microarrays (TMAs) were constructed from 1.50 mm cores of formalin-fixed paraffin-embedded breast tissue. Immunostaining and scoring of the TMAs for CD31, NG2, Hif1a and Met are described in Supplementary Experimental Procedures.

Statistical Analysis

For comparison between two groups, a two-tailed unequal variance *t*-test was used. Association between clinical characteristics and NG2 or Met expression levels was verified

by a two-tailed Fisher's exact test. For survival analysis, Kaplan–Meier curves were drawn and differences between the curves were calculated by the log-rank test. Independent prognostic significance of HIF1α, Met and NG2 was computed by the Cox proportional hazards. *$p \leq 0.05$ was considered statistically significant. All data analysis was performed using R software version 2.13.0 (http://www.R-project.org).

Microarray data: ArrayExpress (Accession number E-MTAB-525).

Supplementary Material

Refer to Web version on PubMed Central for supplementary material.

Acknowledgments

This work was primarily supported by funds from the Champalimaud Foundation for metastasis research, NIH Grants CA125550, CA-155370, CA-151925, DK 081576 and DK 055001. VGC is funded by NRSA F32 Ruth Kirschstein Post-doctoral Fellowship from NIH/NIDDK (5F32DK082119-02). VSL is funded from the NIH Research Training Grant in Gastroenterology (2T32DK007760-11), MBD was funded by the NIH Research Training Grant in Cancer Biology (5T32CA081156-08), a NIH supplemental grant (CA125550) to support diversity, and the United Negro College Fund–Merck Postdoctoral Science Research Fellowship, HS is funded by the NIH Research Training Grant in Cardiovascular Medicine (5T32HL007374-30), JTO is funded by the DoD Breast Cancer Research Predoctoral Traineeship Award (W81XWH-09-1-0008).

References

Acloque H, Adams MS, Fishwick K, Bronner-Fraser M, Nieto MA. Epithelial-mesenchymal transitions: the importance of changing cell state in development and disease. J Clin Invest. 2009; 119:1438–1449. [PubMed: 19487820]

Baba Y, Nosho K, Shima K, Irahara N, Chan AT, Meyerhardt A, Chung DC, Giovannucci EL, Fuchs CS, Ogino S. HIF1A overexpression is associated with poor prognosis in a cohort of 731 colorectal cancers. Am J Pathol. 2010; 176:2292–2301. [PubMed: 20363910]

Bergers G, Song S. The role of pericytes in blood-vessel formation and maintenance. Neuro Oncol. 2005; 7:452–464. [PubMed: 16212810]

Bergers G, Song S, Meyer-Morse N, Bergsland E, Hanahan D. Benefits of targeting both pericytes and endothelial cells in the tumor vasculature with kinase inhibitors. J Clin Invest. 2003; 111:1287–1295. [PubMed: 12727920]

Birchmeier C, Birchmeier W, Gherardi E, Vande Woude GF. Met, metastasis, motility and more. Nat Rev Mol Cell Biol. 2003; 4:915–925. [PubMed: 14685170]

Birner P, Schindl M, Obermair A, Plank C, Breitenecker G, Oberhuber G. Overexpression of hypoxia-inducible factor 1alpha is a marker for an unfavorable prognosis in early-stage invasive cervical cancer. Cancer Res. 2000; 60:4693–4696. [PubMed: 10987269]

Bos R, van der Groep P, Greijer AE, Shvarts A, Meijer S, Pinedo HM, Semenza GL, van Diest PJ, van der Wall E. Levels of hypoxia-inducible factor-1alpha independently predict prognosis in patients with lymph node negative breast carcinoma. Cancer. 2003; 97:1573–1581. [PubMed: 12627523]

Brizel DM, Sibley GS, Prosnitz LR, Scher RL, Dewhirst MW. Tumor hypoxia adversely affects the prognosis of carcinoma of the head and neck. Int J Radiat Oncol Biol Phys. 1997; 38:285–289. [PubMed: 9226314]

Carmeliet P, Jain RK. Principles and mechanisms of vessel normalization for cancer and other angiogenic diseases. Nat Rev Drug Discov. 2011; 10:417–427. [PubMed: 21629292]

Chen J, Imanaka N, Griffin JD. Hypoxia potentiates Notch signaling in breast cancer leading to decreased E-cadherin expression and increased cell migration and invasion. Br J Cancer. 2010; 102:351–360. [PubMed: 20010940]

Coussens LM, Tinkle CL, Hanahan D, Werb Z. MMP-9 supplied by bone marrow-derived cells contributes to skin carcinogenesis. Cell. 2000; 103:481–490. [PubMed: 11081634]

Dachs GU, Tozer GM. Hypoxia modulated gene expression: angiogenesis, metastasis and therapeutic exploitation. Eur J Cancer. 2000; 36:1649–1660. [PubMed: 10959051]

Di Renzo MF, Narsimhan RP, Olivero M, Bretti S, Giordano S, Medico E, Gaglia P, Zara P, Comoglio PM. Expression of the Met/HGF receptor in normal and neoplastic human tissues. Oncogene. 1991; 6:1997–2003. [PubMed: 1719465]

Di Renzo MF, Olivero M, Giacomini A, Porte H, Chastre E, Mirossay L, Nordlinger B, Bretti S, Bottardi S, Giordano S, et al. Overexpression and amplification of the met/HGF receptor gene during the progression of colorectal cancer. Clin Cancer Res. 1995; 1:147–154. [PubMed: 9815967]

Dore-Duffy P. Pericytes: pluripotent cells of the blood brain barrier. Curr Pharm Des. 2008; 14:1581–1593. [PubMed: 18673199]

Dore-Duffy P, Cleary K. Morphology and properties of pericytes. Methods Mol Biol. 2011; 686:49–68. [PubMed: 21082366]

Eberhard A, Kahlert S, Goede V, Hemmerlein B, Plate KH, Augustin HG. Heterogeneity of angiogenesis and blood vessel maturation in human tumors: implications for antiangiogenic tumor therapies. Cancer Res. 2000; 60:1388–1393. [PubMed: 10728704]

Ebos JM, Lee CR, Cruz-Munoz W, Bjarnason GA, Christensen JG, Kerbel RS. Accelerated metastasis after short-term treatment with a potent inhibitor of tumor angiogenesis. Cancer Cell. 2009; 15:232–239. [PubMed: 19249681]

Eckerich C, Zapf S, Fillbrandt R, Loges S, Westphal M, Lamszus K. Hypoxia can induce c-Met expression in glioma cells and enhance SF/HGF-induced cell migration. Int J Cancer. 2007; 121:276–283. [PubMed: 17372907]

Erler JT, Bennewith KL, Nicolau M, Dornhofer N, Kong C, Le QT, Chi T, Jeffrey SS, Giaccia AJ. Lysyl oxidase is essential for hypoxia-induced metastasis. Nature. 2006; 440:1222–1226. [PubMed: 16642001]

Folkman J. Tumor angiogenesis: therapeutic implications. N Engl J Med. 1971; 285:1182–1186. [PubMed: 4938153]

Folkman J. Tumor angiogenesis. Adv Cancer Res. 1974; 19:331–358. [PubMed: 4605404]

Folkman J. Angiogenesis in cancer, vascular, rheumatoid and other disease. Nat Med. 1995; 1:27–31. [PubMed: 7584949]

Garcia S, Dales JP, Charafe-Jauffret E, Carpentier-Meunier S, Andrac-Meyer L, Jacquemier J, Andonian C, Lavaut MN, Allasia C, Bonnier P, Charpin C. Poor prognosis in breast carcinomas correlates with increased expression of targetable CD146 and c-Met and with proteomic basal-like phenotype. Hum Pathol. 2007; 38:830–841. [PubMed: 17316758]

Gupta GP, Massague J. Cancer metastasis: building a framework. Cell. 2006; 127:679–695. [PubMed: 17110329]

Hanahan D, Weinberg RA. The hallmarks of cancer. Cell. 2000; 100:57–70. [PubMed: 10647931]

Hara S, Nakashiro K, Klosek SK, Ishikawa T, Shintani S, Hamakawa H. Hypoxia enhances c-Met/HGF receptor expression and signaling by activating HIF-1alpha in human salivary gland cancer cells. Oral Oncol. 2006; 42:593–598. [PubMed: 16469527]

Harris AL. Hypoxia--a key regulatory factor in tumour growth. Nat Rev Cancer. 2002; 2:38–47. [PubMed: 11902584]

Hayashi M, Sakata M, Takeda T, Tahara M, Yamamoto T, Okamoto Y, Minekawa R, Isobe A, Ohmichi M, Tasaka K, Murata Y. Up-regulation of c-met protooncogene product expression through hypoxia-inducible factor-1alpha is involved in trophoblast invasion under low-oxygen tension. Endocrinology. 2005; 146:4682–4689. [PubMed: 16099863]

Hellstrom M, Kalen M, Lindahl P, Abramsson A, Betsholtz C. Role of PDGF-B and PDGFR-beta in recruitment of vascular smooth muscle cells and pericytes during embryonic blood vessel formation in the mouse. Development. 1999; 126:3047–3055. [PubMed: 10375497]

Huang FJ, You WK, Bonaldo P, Seyfried TN, Pasquale EB, Stallcup WB. Pericyte deficiencies lead to aberrant tumor vascularizaton in the brain of the NG2 null mouse. Dev Biol. 2010; 344:1035–1046. [PubMed: 20599895]

Jain RK. Transport of molecules in the tumor interstitium: a review. Cancer Res. 1987; 47:3039–3051. [PubMed: 3555767]

Jain RK. Molecular regulation of vessel maturation. Nat Med. 2003; 9:685–693. [PubMed: 12778167]

Joyce JA. Therapeutic targeting of the tumor microenvironment. Cancer Cell. 2005; 7:513–520. [PubMed: 15950901]

Kalluri R. EMT: when epithelial cells decide to become mesenchymal-like cells. J Clin Invest. 2009; 119:1417–1419. [PubMed: 19487817]

Kalluri R, Weinberg RA. The basics of epithelial-mesenchymal transition. J Clin Invest. 2009; 119:1420–1428. [PubMed: 19487818]

Kenworthy P, Dowrick P, Baillie-Johnson H, McCann B, Tsubouchi H, Arakaki N, Daikuhara Y, Warn RM. The presence of scatter factor in patients with metastatic spread to the pleura. Br J Cancer. 1992; 66:243–247. [PubMed: 1387000]

Kim JA, Tran ND, Li Z, Yang F, Zhou W, Fisher MJ. Brain endothelial hemostasis regulation by pericytes. J Cereb Blood Flow Metab. 2006; 26:209–217. [PubMed: 16015279]

Koukourakis MI, Giatromanolaki A, Sivridis E, Simopoulos C, Turley H, Talks K, Gatter KC, Harris AL. Hypoxia-inducible factor (HIF1A and HIF2A), angiogenesis, and chemoradiotherapy outcome of squamous cell head-and-neck cancer. Int J Radiat Oncol Biol Phys. 2002; 53:1192–1202. [PubMed: 12128120]

Liebner S, Fischmann A, Rascher G, Duffner F, Grote EH, Kalbacher H, Wolburg H. Claudin-1 and claudin-5 expression and tight junction morphology are altered in blood vessels of human glioblastoma multiforme. Acta Neuropathol. 2000; 100:323–331. [PubMed: 10965803]

Lu C, Kamat AA, Lin YG, Merritt WM, Landen CN, Kim TJ, Spannuth W, Arumugam T, Han LY, Jennings NB, et al. Dual targeting of endothelial cells and pericytes in antivascular therapy for ovarian carcinoma. Clin Cancer Res. 2007; 13:4209–4217. [PubMed: 17634550]

Lu C, Shahzad MM, Moreno-Smith M, Lin YG, Jennings NB, Allen JK, Landen CN, Mangala LS, Armaiz-Pena GN, Schmandt R, et al. Targeting pericytes with a PDGF-B aptamer in human ovarian carcinoma models. Cancer Biol Ther. 2010; 9:176–182. [PubMed: 20009575]

Mendel DB, Laird AD, Xin X, Louie SG, Christensen JG, Li G, Schreck RE, Abrams TJ, Ngai TJ, Lee LB, et al. In vivo antitumor activity of SU11248, a novel tyrosine kinase inhibitor targeting vascular endothelial growth factor and platelet-derived growth factor receptors: determination of a pharmacokinetic/pharmacodynamic relationship. Clin Cancer Res. 2003; 9:327–337. [PubMed: 12538485]

Motzer RJ, Hutson TE, Tomczak P, Michaelson MD, Bukowski RM, Rixe O, Oudard S, Negrier S, Szczylik C, Kim ST, et al. Sunitinib versus interferon alfa in metastatic renal-cell carcinoma. N Engl J Med. 2007; 356:115–124. [PubMed: 17215529]

Munoz-Najar UM, Neurath KM, Vumbaca F, Claffey KP. Hypoxia stimulates breast carcinoma cell invasion through MT1-MMP and MMP-2 activation. Oncogene. 2006; 25:2379–2392. [PubMed: 16369494]

Natali PG, Nicotra MR, Di Renzo MF, Prat M, Bigotti A, Cavaliere R, Comoglio PM. Expression of the c-Met/HGF receptor in human melanocytic neoplasms: demonstration of the relationship to malignant melanoma tumour progression. Br J Cancer. 1993; 68:746–750. [PubMed: 8104462]

Newman PJ. The role of PECAM-1 in vascular cell biology. Ann N Y Acad Sci. 1994; 714:165–174. [PubMed: 8017765]

O'Keeffe MB, Devlin AH, Burns AJ, Gardiner TA, Logan ID, Hirst DG, McKeown SR. Investigation of pericytes, hypoxia, and vascularity in bladder tumors: association with clinical outcomes. Oncol Res. 2008; 17:93–101. [PubMed: 18669161]

Ozerdem U. Targeting of pericytes diminishes neovascularization and lymphangiogenesis in prostate cancer. Prostate. 2006a; 66:294–304. [PubMed: 16245280]

Ozerdem U. Targeting pericytes diminishes neovascularization in orthotopic uveal melanoma in nerve/glial antigen 2 proteoglycan knockout mouse. Ophthalmic Res. 2006b; 38:251–254. [PubMed: 16888406]

Ozerdem U, Freeman WR, Bartsch DU, Clark TM. A simple noncontact wide-angle fundus photography procedure for clinical and research use. Retina. 2001a; 21:189–190. [PubMed: 11321153]

Ozerdem U, Grako KA, Dahlin-Huppe K, Monosov E, Stallcup WB. NG2 proteoglycan is expressed exclusively by mural cells during vascular morphogenesis. Dev Dyn. 2001b; 222:218–227. [PubMed: 11668599]

Ozerdem U, Monosov E, Stallcup WB. NG2 proteoglycan expression by pericytes in pathological microvasculature. Microvasc Res. 2002; 63:129–134. [PubMed: 11749079]

Paez-Ribes M, Allen E, Hudock J, Takeda T, Okuyama H, Vinals F, Inoue M, Bergers G, Hanahan D, Casanovas O. Antiangiogenic therapy elicits malignant progression of tumors to increased local invasion and distant metastasis. Cancer Cell. 2009; 15:220–231. [PubMed: 19249680]

Pennacchietti S, Michieli P, Galluzzo M, Mazzone M, Giordano S, Comoglio PM. Hypoxia promotes invasive growth by transcriptional activation of the met protooncogene. Cancer Cell. 2003; 3:347–361. [PubMed: 12726861]

Pietras K, Hanahan D. A multitargeted, metronomic, and maximum-tolerated dose "chemo-switch" regimen is antiangiogenic, producing objective responses and survival benefit in a mouse model of cancer. J Clin Oncol. 2005; 23:939–952. [PubMed: 15557593]

Pouyssegur J, Dayan F, Mazure NM. Hypoxia signalling in cancer and approaches to enforce tumour regression. Nature. 2006; 441:437–443. [PubMed: 16724055]

Qian F, Engst S, Yamaguchi K, Yu P, Won KA, Mock L, Lou T, Tan J, Li C, Tam D, et al. Inhibition of tumor cell growth, invasion, and metastasis by EXEL-2880 (XL880, GSK1363089), a novel inhibitor of HGF and VEGF receptor tyrosine kinases. Cancer Res. 2009; 69:8009–8016. [PubMed: 19808973]

Raza A, Franklin MJ, Dudek AZ. Pericytes and vessel maturation during tumor angiogenesis and metastasis. Am J Hematol. 2010; 85:593–598. [PubMed: 20540157]

Rofstad EK. Microenvironment-induced cancer metastasis. Int J Radiat Biol. 2000; 76:589–605. [PubMed: 10866281]

Schlingemann RO, Rietveld FJ, de Waal RM, Ferrone S, Ruiter DJ. Expression of the high molecular weight melanoma-associated antigen by pericytes during angiogenesis in tumors and in healing wounds. Am J Pathol. 1990; 136:1393–1405. [PubMed: 1694058]

Semenza GL. Angiogenesis in ischemic and neoplastic disorders. Annu Rev Med. 2003; 54:17–28. [PubMed: 12359828]

Sennino B, Falcon BL, McCauley D, Le T, McCauley T, Kurz JC, Haskell A, Epstein DM, McDonald DM. Sequential loss of tumor vessel pericytes and endothelial cells after inhibition of platelet-derived growth factor B by selective aptamer AX102. Cancer Res. 2007; 67:7358–7367. [PubMed: 17671206]

Stefansson IM, Salvesen HB, Akslen LA. Vascular proliferation is important for clinical progress of endometrial cancer. Cancer Res. 2006; 66:3303–3309. [PubMed: 16540684]

Stohrer M, Boucher Y, Stangassinger M, Jain RK. Oncotic pressure in solid tumors is elevated. Cancer Res. 2000; 60:4251–4255. [PubMed: 10945638]

Sugimoto H, Mundel TM, Kieran MW, Kalluri R. Identification of fibroblast heterogeneity in the tumor microenvironment. Cancer Biol Ther. 2006; 5:1640–1646. [PubMed: 17106243]

Sun S, Ning X, Zhang Y, Lu Y, Nie Y, Han S, Liu L, Du R, Xia L, He L, Fan D. Hypoxia-inducible factor-1alpha induces Twist expression in tubular epithelial cells subjected to hypoxia, leading to epithelial-to-mesenchymal transition. Kidney Int. 2009; 75:1278–1287. [PubMed: 19279556]

Thiery JP. [Epithelial-mesenchymal transitions in cancer onset and progression]. Bull Acad Natl Med. 2009; 193:1969–1978. discussion 1978-1969. [PubMed: 20666011]

Thiery JP, Acloque H, Huang RY, Nieto MA. Epithelial-mesenchymal transitions in development and disease. Cell. 2009; 139:871–890. [PubMed: 19945376]

Tong RT, Boucher Y, Kozin SV, Winkler F, Hicklin DJ, Jain RK. Vascular normalization by vascular endothelial growth factor receptor 2 blockade induces a pressure gradient across the vasculature and improves drug penetration in tumors. Cancer Res. 2004; 64:3731–3736. [PubMed: 15172975]

Trimboli AJ, Fukino K, de Bruin A, Wei G, Shen L, Tanner SM, Creasap N, Rosol TJ, Robinson ML, Eng C, et al. Direct evidence for epithelial-mesenchymal transitions in breast cancer. Cancer Res. 2008; 68:937–945. [PubMed: 18245497]

Vleugel MM, Greijer AE, Shvarts A, van der Groep P, van Berkel M, Aarbodem Y, van Tinteren H, Harris AL, van Diest PJ, van der Wall E. Differential prognostic impact of hypoxia induced and

diffuse HIF-1alpha expression in invasive breast cancer. J Clin Pathol. 2005; 58:172–177. [PubMed: 15677538]

Xian X, Hakansson J, Stahlberg A, Lindblom P, Betsholtz C, Gerhardt H, Semb H. Pericytes limit tumor cell metastasis. J Clin Invest. 2006; 116:642–651. [PubMed: 16470244]

Xie X, Huang S. Regulation of cancer metastasis by stress pathways. Clin Exp Metastasis. 2003; 20:31–43. [PubMed: 12650605]

Xie L, Duncan MB, Pahler J, Sugimoto H, Martino M, Lively J, Mundel T, Soubasakos M, Rubin K, Takeda T, et al. Counterbalancing angiogenic regulatory factors control the rate of cancer progression and survival in a stage-specific manner. Proc Natl Acad Sci U S A. 2011; 108:9939–9944. [PubMed: 21622854]

Yang J, Mani SA, Donaher JL, Ramaswamy S, Itzykson RA, Come C, Savagner P, Gitelman I, Richardson A, Weinberg RA. Twist, a master regulator of morphogenesis, plays an essential role in tumor metastasis. Cell. 2004; 117:927–939. [PubMed: 15210113]

Yang MH, Wu MZ, Chiou SH, Chen PM, Chang SY, Liu CJ, Teng SC, Wu KJ. Direct regulation of TWIST by HIF-1alpha promotes metastasis. Nat Cell Biol. 2008; 10:295–305. [PubMed: 18297062]

Yonenaga Y, Mori A, Onodera H, Yasuda S, Oe H, Fujimoto A, Tachibana T, Imamura M. Absence of smooth muscle actin-positive pericyte coverage of tumor vessels correlates with hematogenous metastasis and prognosis of colorectal cancer patients. Oncology. 2005; 69:159–166. [PubMed: 16127287]

You WK, Sennino B, Williamson CW, Falcon B, Hashizume H, Yao LC, Aftab DT, McDonald DM. VEGF and c-Met blockade amplify angiogenesis inhibition in pancreatic islet cancer. Cancer Res. 2011; 71:4758–4768. [PubMed: 21613405]

Zou HY, Li Q, Lee JH, Arango ME, McDonnell SR, Yamazaki S, Koudriakova TB, Alton G, Cui JJ, Kung PP, et al. An orally available small-molecule inhibitor of c-Met, PF-2341066, exhibits cytoreductive antitumor efficacy through antiproliferative and antiangiogenic mechanisms. Cancer Res. 2007; 67:4408–4417. [PubMed: 17483355]

Significance

Pericyte coverage and its relation to metastasis are poorly understood. This study suggests that pericyte coverage on tumor vasculature serves as a key negative regulator of metastasis. Clinical studies suggest that cancer patients with low numbers of vessel-associated pericytes exhibit a high mortality rate. Cancer cell autonomous changes cooperate with stromal changes to determine the rate of cancer progression and metastasis.

Highlights

- Pericyte loss increases tumor hypoxia, HIF1α and Met expression, EMT and metastasis
- Pharmacological targeting of pericytes or Met inhibits EMT and reduces metastasis
- Reduced pericytes and Met overexpression correlate with poor patient prognosis
- Cancer cell-autonomous program and stromal alterations combine to support metastasis

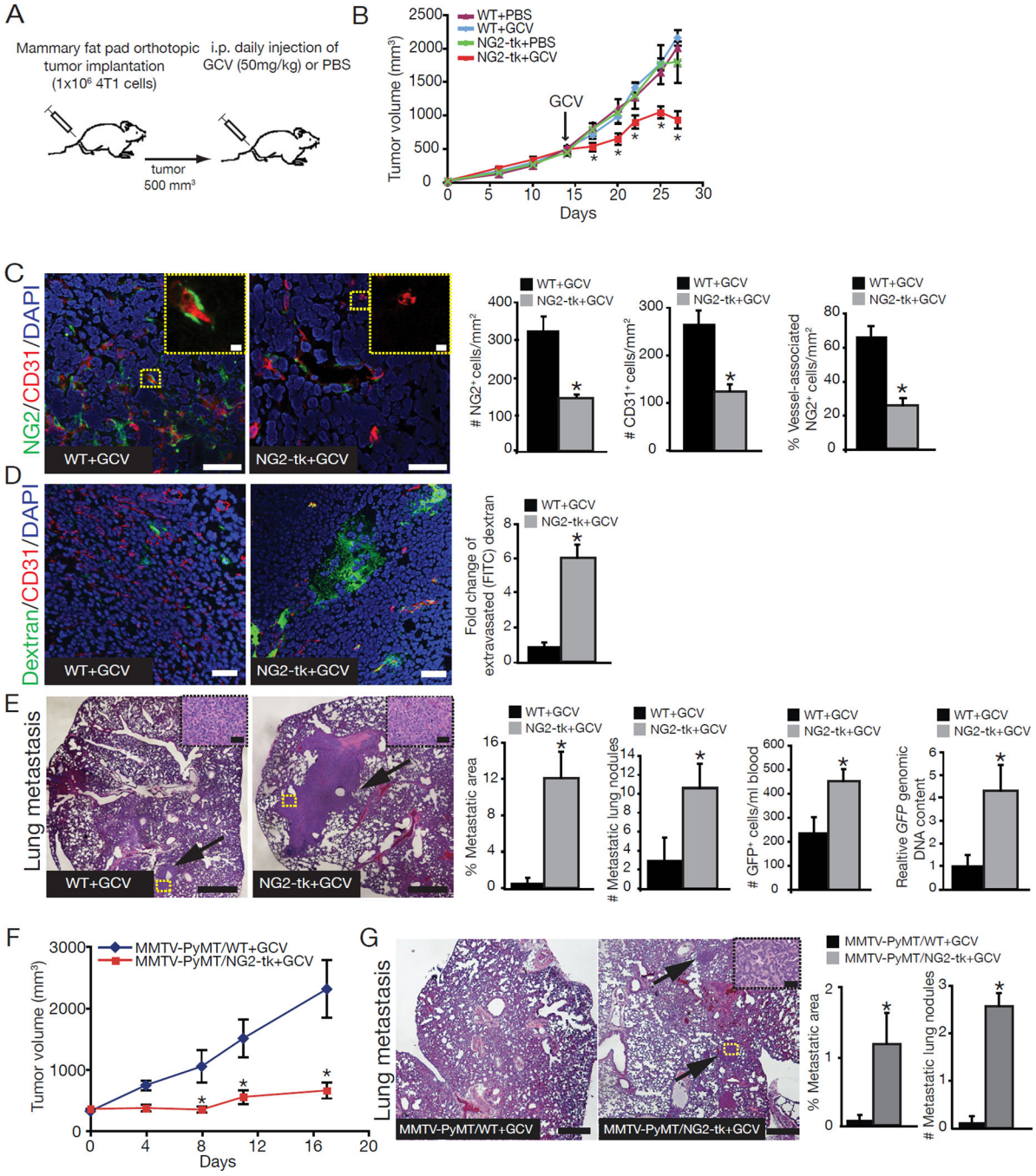

Figure 1. Reduced tumor growth and increased metastasis after depletion of vessel-associated NG2$^+$ cells

(A) Orthotopic implantation of 4T1 cancer cells in NG2-tk mice and wildtype littermates, with daily ganciclovir (GCV) or saline (PBS) injections beginning when tumors reached ~500mm^3. **(B)** Tumor volumes over the experimental timecourse. **(C)** Representative images of tumor sections from WT+GCV and NG2-tk+GCV mice immunolabeled for NG2 (green)/CD31 (red), and quantification of number of NG2$^+$ cells, CD31$^+$ cells, and percent vessel-associated NG2$^+$ cells in each group. DAPI=nuclei. Scale bar: 50μm. High magnification images are located in the upper right corner. Scale bar: 10μm. **(D)** Representative images of tumor sections immunolabeled for CD31 (red) and quantitative analysis of extravascular FITC-dextran. DAPI=nuclei. Scale bar: 50μm. **(E)** Representative images of H&E-stained lung sections. Scale bar: 10μm. Arrows

point to metastatic nodules. High magnification images of metastatic nodules are located in the upper right corner. Scale bar: 50μm. Percent metastatic area, number of metastatic lung nodules, number of 4T1-GFP$^+$ cells in the blood, and relative GFP content in lungs of NG2-tk+GCV mice compared to WT+GCV mice. **(F)** MMTV-PyMT/WT and MMTV-PyMT/NG2-tk female mice were treated with GCV when tumors reached ~500mm^3 and tumor volumes measurements over time. **(G)** Representative images of H&E-stained lung sections of MMTV-PyMT/WT+GCV and MMTV-PyMT/NG2-tk+GCV mice. Scale bar: 10μm. Arrows point to metastatic nodules. Percent metastatic area and number of metastatic lung nodules. Error bars display SEM; asterisks denote significance (*$p<0.05$). NS: non-significant. See also Figure S1 and Table S1.

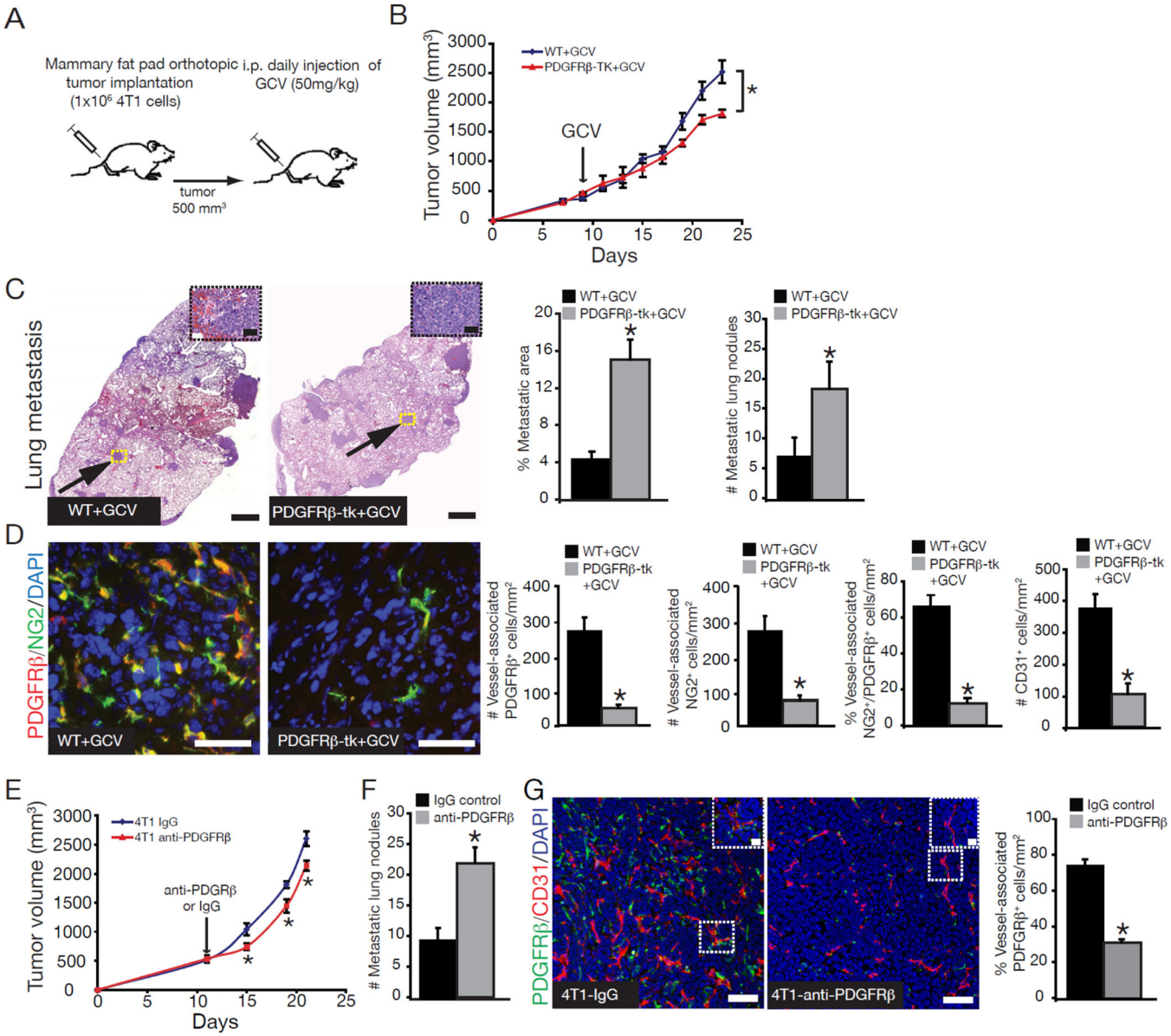

Figure 2. Reduced tumor growth and increased metastasis after depletion of vessel-associated PDGFRβ$^+$ cells

(A) Orthotopic implantation of 4T1 cancer cells into PDGFRβ-tk mice and wildtype littermates, with daily ganciclovir (GCV) injections beginning when tumors reached ~500mm^3. **(B)** Tumor volumes over the experimental timecourse. **(C)** Representative images of H&E-stained lung sections. Scale bar: 10μm. Arrows point to metastatic areas. High magnification images of metastatic nodules are located in the upper right corner. Scale bar: 50μm Percent metastatic area and number of metastatic lung nodules. **(D)** Representative images of immunostaining for PDGFRβ (red) and NG2 (green) tumor sections. DAPI=nuclei. Scale bar: 50μm. Quantitative assessment of vessel-associated PDGFRβ$^+$, NG2$^+$, PDGFRβ$^+$/NG2$^+$ double positive, and CD31$^+$ cells in 4T1 tumors from PDGFRβ-tk+GCV and WT+GCV mice. **(E)** Tumor volumes over the experimental timecourse in mice treated with anti-PDGFRβ antibody or control IgG. **(F)** Number of metastatic lung nodules. **(G)** Representative images of tumor sections immunolabeled for PDGFRβ (green)/CD31 (red) in IgG-treated and anti- PDGFRβ-treated mice, and quantification of vessel-associated PDGFRβ$^+$ cells in the tumors, scale bar: 50μm. Inserts are magnified images of selected area, scale bar: scale bar: 10μm. Error bars display SEM; *p<0.05. See also Figure S2.

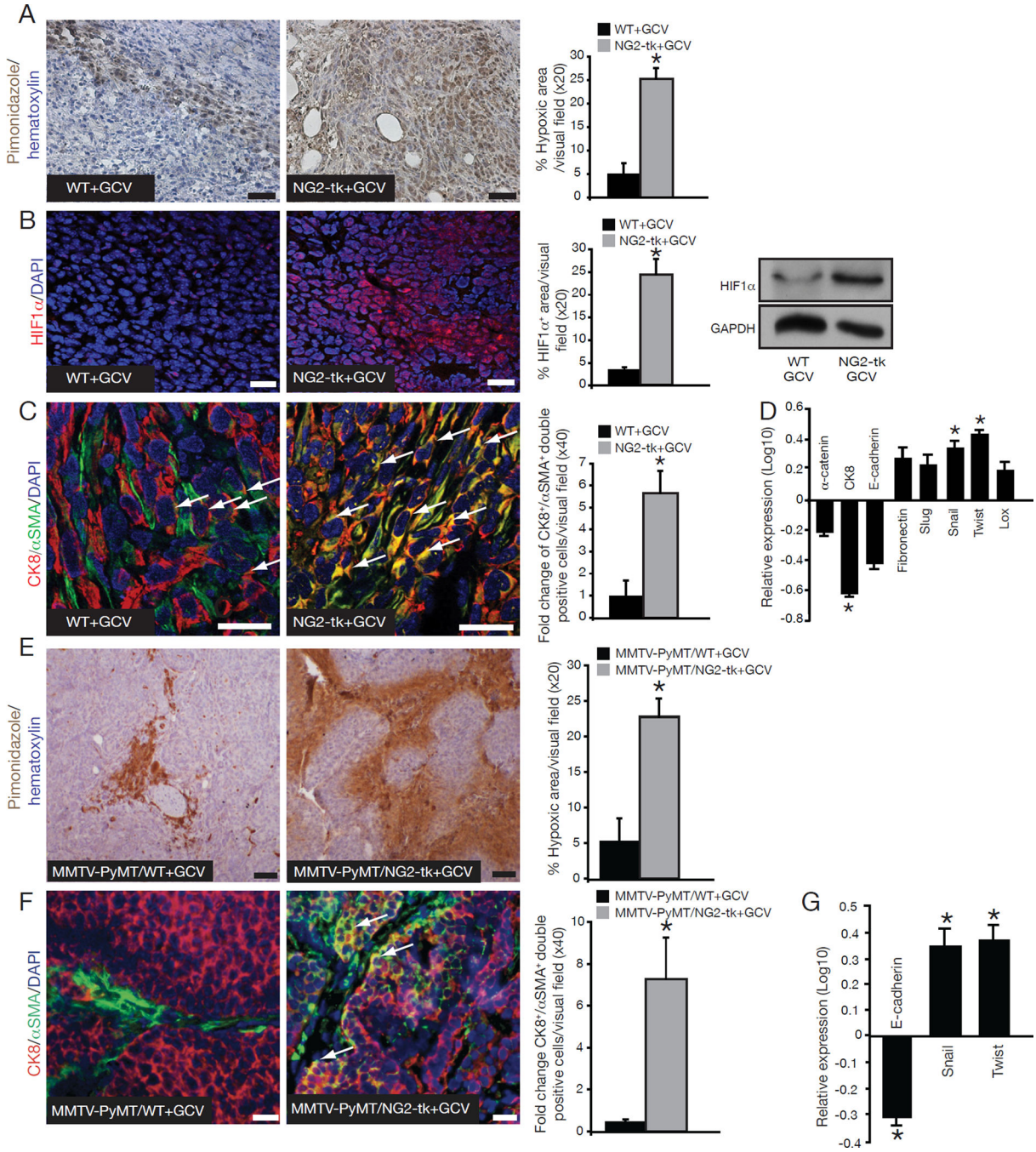

Figure 3. Increase in hypoxia and EMT in pericyte-depleted tumors

(A) Hypoxia was detected by immunohistochemistry staining of pimonidazole adducts in 4T1 tumor sections from NG2-tk +GCV and WT+GCV mice. Nuclear counterstain: hematoxylin stain. Quantitative analysis of the percent hypoxic area per visual field. **(B)** Immunostaining for HIF1α. DAPI=nuclei. Quantification of HIF1α immunostaning and Western blot analysis for HIF1α expression; GAPDH is used as an internal control. **(C)** EMT as detected by immunofluorescent staining for Cytokeratin 8 (red) and αSMA (green). DAPI=nuclei. Arrows point to $CK8^+/\alpha SMA^+$ double-positive cells. Quantification of EMT is plotted as fold change in the number of $CK8^+/\alpha SMA^+$ double-positive cells per visual field. **(D)** Quantitative RT-PCR for α-*catenin, Cytokeratin 8 (CK8), E-cadherin, Fibronectin, Slug, Snail, Twist, and Lox* comparing expression levels in tumor

tissues from NG2-tk+GCV mice relative to WT+GCV mice and plotted as log10 relative expression. **(E)** Representative images of pimonidazole adducts staining (hypoxia). Nuclear counterstain: hematoxylin staining. Quantification of the percent hypoxic area per visual field. **(F)** EMT as detected by immunofluorescent staining for Cytokeratin 8 (red) and αSMA (green). DAPI=nuclei. Arrows point to $CK8^+/\alpha SMA^+$ double-positive cells. Quantification of EMT plotted as the number of $CK8^+/\alpha SMA^+$ double-positive cells per visual field. **(G)** Quantitative RT-PCR for *E-cadherin, Snail, and Twist* plotted as log10 relative expression. Error bars display SEM; asterisks denote significance (*$p<0.05$). Scale bar: 50 μm. See also Tables S2–4.

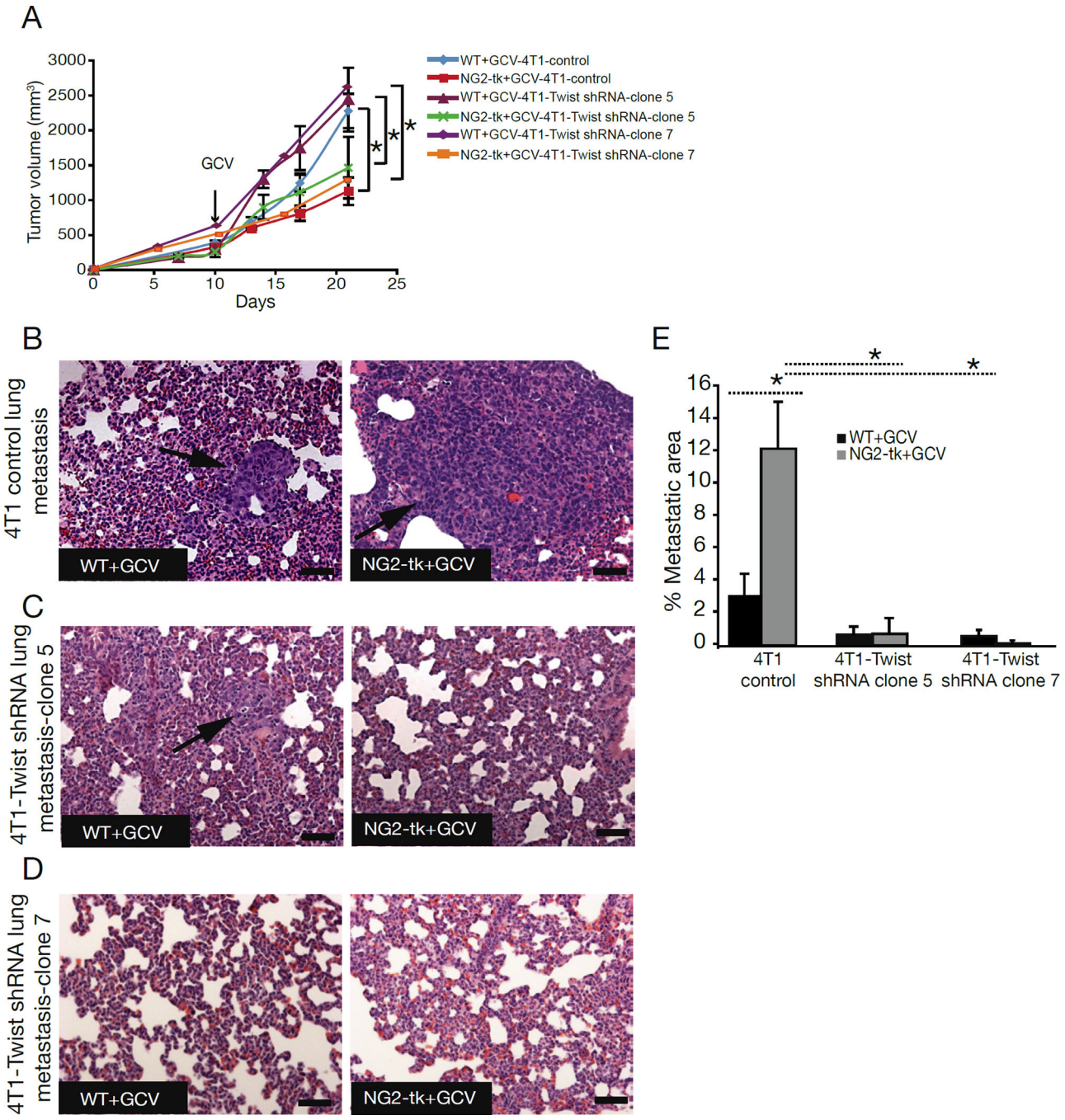

Figure 4. Decreased metastasis in mice with pericyte-depleted tumors after inhibition of EMT

(A) Tumor volumes over the experimental timecourse in WT+GCV and NG2-tk+GCV mice implanted with 4T1 or 4T1-Twist shRNA cells. **(B–D)** Representative photomicrographs of H&E-stained lung sections of WT+GCV and NG2-tk+GCV mice implanted with **(B)** 4T1 cells, **(C)** 4T1-Twist shRNA cells-clone 5 and **(D)** 4T1-Twist shRNA cells-clone 7. Arrows point to metastatic nodules. **(E)** Quantification of metastatic area. Error bars display SEM; asterisks denote significance (*p<0.05). NS: non-significant. Scale bar: 50 μm.

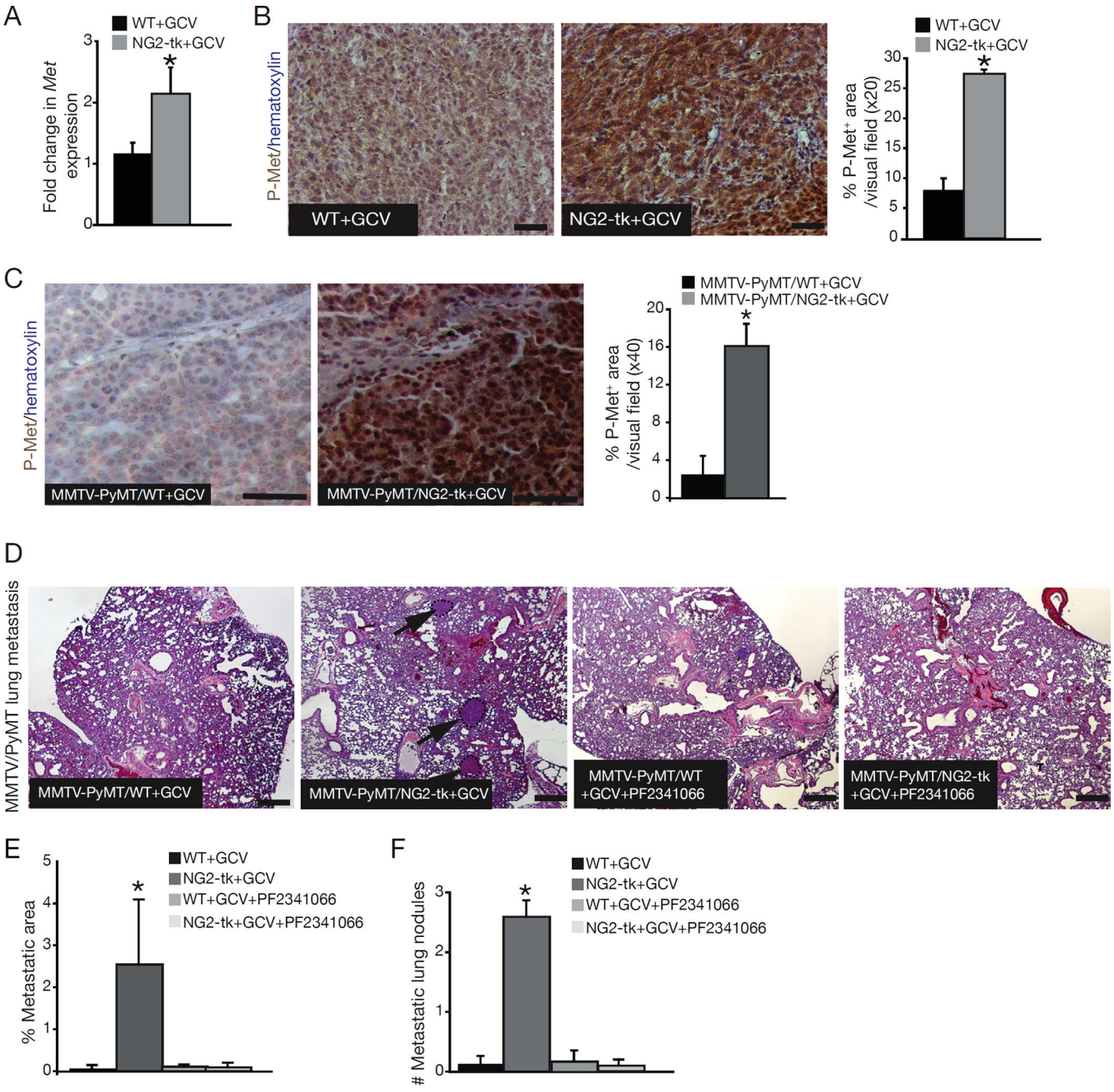

Figure 5. Suppression of metastasis in pericyte-ablated mice after Met inhibition

(A) Quantitative RT-PCR for *Met* mRNA expression in tumors from NG2-tk+GCV and WT+GCV mice. **(B)** Immunostaining of 4T1 tumor for phosphorylated Met (p-Met). Nuclear counterstain: hematoxylin. Scale bar: 50 μm. Quantification of p-Met expression. **(C)** Immunostaining and quantification of p-Met (mammary tumors). Nuclear counterstai: hematoxylin. Scale bar: 50 μm. **(D)** Representative images of H&E-stained lung sections from MMTV-PyMT/WT and MMTVPyMT/ NG2-tk mice treated with GCV or GCV+PF2341066. Arrows point to metastatic nodules. Scale bar: 50 μm. **(E)** Percent lung metastatic area. **(F)** Number of metastatic lung nodules before and after PF2341066 treatment. Error bars display SEM; asterisks denote significance (*$p<0.05$). Scale bar: 50 μm. See also Figure S4.

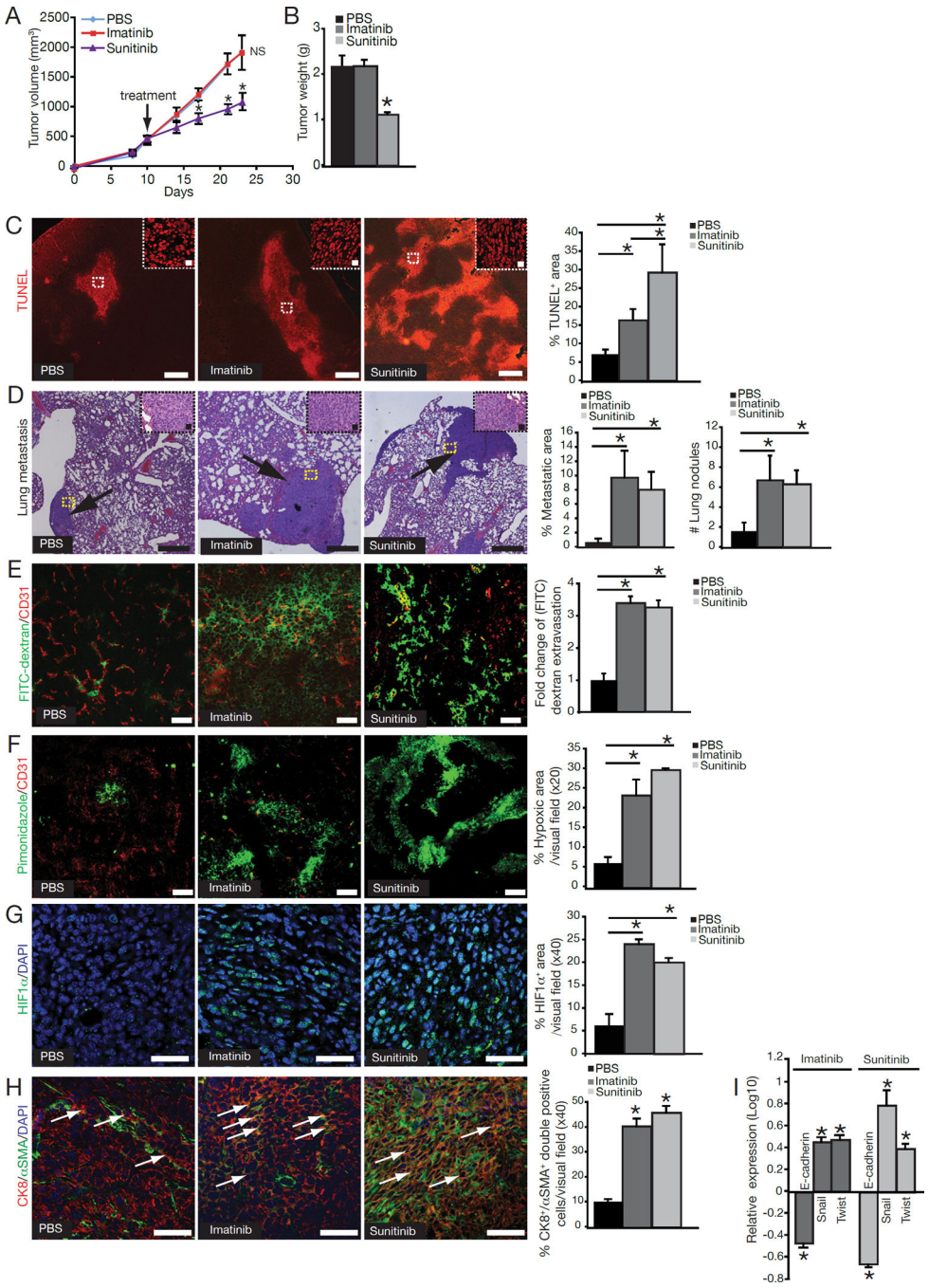

Figure 6. Decreased pericyte coverage, altered vasculature, enhanced EMT, and increased metastasis in Imatinib- and Sunitinib-treated mice

(A) Orthotopic implantation of 4T1 cancer cells into PBS-, Imatinib- and Sunitinib-treated mice and tumor volumes over the experimental timecourse. **(B)** Tumor weight at the experimental endpoint. **(C)** Representative images of TUNEL immunofluorescent labeling and quantification of the percent TUNEL^{+} area per visual field. Scale bar: 10 μm. High magnification images are shown in the upper right corner. Scale bar: 50 μm. **(D)** Representative photomicrographs of H&Estained lung sections of control and treated mice. Scale bar: 10 μm. Arrows point to metastatic areas. High magnification images of metastatic nodules are located in the upper right corner. Scale bar: 50 μm. Percent metastatic area and number of

metastatic lung nodules. **(E)** Representative images and quantitative analysis of extravascular FITC-dextran. Scale bar: 50 μm. **(F)** Representative immunofluorescent images of staining for pimonidazole adducts in tumor sections and quantification. Scale bar: 50 μm. **(G)** Representative immunofluorescent images and quantification of HIF1α expression. DAPI=nuclei. Scale bar: 50 μm. **(H)** EMT was detected in 4T1 tumors of control and treated mice by immunofluorescent staining for Cytokeratin 8 (red) and αSMA (green). DAPI=nuclei. Arrows point to $CK8^+/\alpha SMA^+$ double-positive cells. Scale bar: 50 μm. Quantification of EMT plotted as percent of $CK8^+/\alpha SMA^+$ double-positive cells per visual field. **(I)** Quantitative RT-PCR analysis for *E-cadherin, Snail, and Twist* mRNA expression from tumor tissues of control and treated mice and plotted as log10 relative expression. Error bars display SEM; asterisks denote significance (*$p<0.05$). NS: non-significant. See also Figure S3.

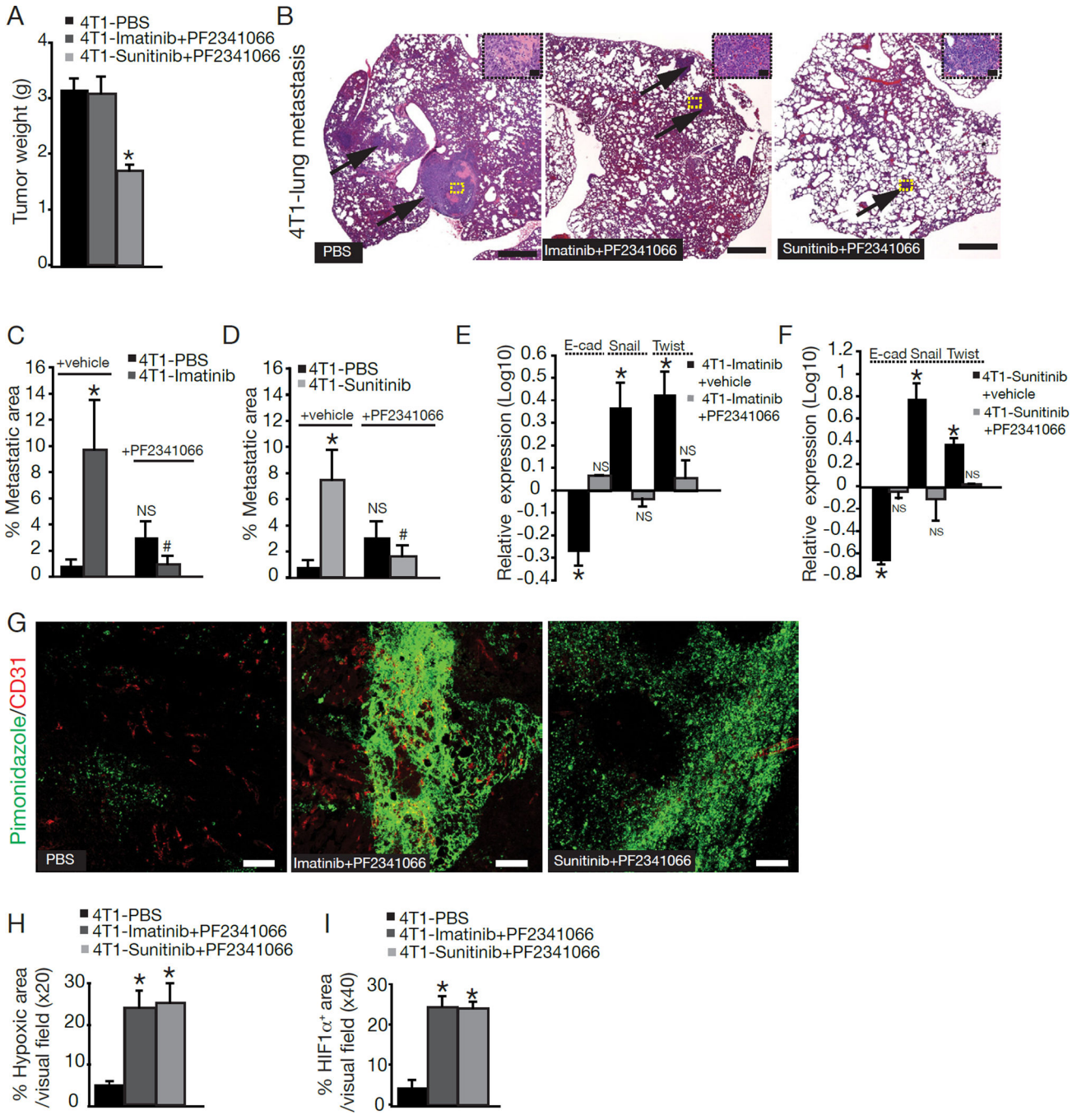

Figure 7. Suppression of metastasis in Imatinib-treated and Sunitinibtreated mice after Met inhibition

(A) 4T1 tumor weight after drug treatment. **(B)** Representative images of H&E-stained lung sections from tumor-bearing mice treated with PBS, Imatinib+PF2341066, or Sunitinib+PF2341066. Arrows point to metastatic nodules. Scale bar: 10 μm. High magnification images of metastatic nodules are located in the upper right corner. Scale bar: 50 μm. **(C–D)** Quantification of percent metastatic area in the lungs of these mice. Significance ($p<0.05$) is denoted by * when comparing PBS+vehicle-treated mice *vs*. Imatinib/Sunitinib+vehicle-treated mice and by # when comparing Imatinib/Sunitinib+vehicle-treated mice *vs*. Imatinib/Sunitinib+PF2341066-treated mice. **(E–F)** Quantitative RT-PCR for *E-cadherin*, *Twist*, and *Snail* in tumor tissues from Imatinib-treated mice with and without PF2341066 treatment. **(G)** Hypoxia was detected by immunofluorescent staining of

pimonidazole adducts in tumor sections after PF2341066 treatment. Scale bar: 50 μ. **(H)** Quantitative analysis of pimonidazole accumulation. **(I)** Quantitative analysis of HIF1α expression. Error bars display SEM; asterisks denote significance (*p<0.05). NS: non-significant. See also Figure S4.

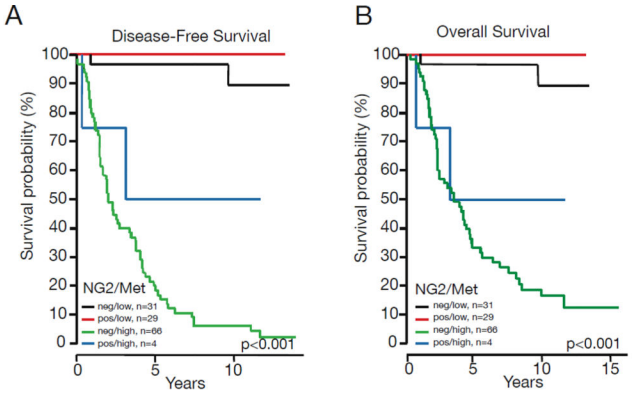

C

Clinical Characteristics

Variable	Number of patients (n=130), median age (range)-59yrs (26-96)				p value
	NG2 neg (n=97)		NG2 pos (n=33)		
	low Met (n=31)	high Met (n=66)	low Met (n=29)	high Met (n=4)	
Tumor size					0.043
<2.0cm	4	1	2	0	
2.0 to <5.0cm	18	37	21	1	
<or= 5.0cm	7	26	5	2	
unknown	2	2	1	1	
Stage					0.019
I	1	0	0	0	
IIA	9	13	14	0	
IIB	1	2	2	0	
IIIA	0	1	0	1	
IIIB	20	50	13	3	
IV	0	0	0	0	
Depth of invasion					0.009
pT1	3	0	2	0	
pT2	7	14	14	0	
pT3	0	1	0	0	
pT4	19	51	13	4	
pTX	2	0	0	0	
Lymph node metastasis					0.205
pN0	16	23	16	2	
pN1	11	25	8	0	
pN2	4	18	5	2	
Distant metastasis					<0.001
Yes	2	63	0	2	
No	29	3	29	2	

Figure 8. Poor pericyte coverage and high Met expression is correlated with decreased survival of breast cancer patients

(A) Disease-free and **(B)** overall survival of invasive ductal carcinoma (IDC) patients with relation to $CD31^+$ vessel-associated NG2 expression together with Met expression. **(C)** Baseline demographics and clinical characteristics associated with $CD31^+$ vessel-associated NG2 expression and Met expression.